Shape and size transformations of biomass particles during combustion

Juan Riaza[1], Patrick Mason[2], Jenny M. Jones[2], Alan Williams[2], Jon Gibbins[1, 3], Hannah Chalmers[1*]

1 Institute for Energy Systems, School of Engineering, University of Edinburgh. The King's Buildings, Mayfield Road, Edinburgh, EH93JL, Scotland, UK

2 School of Chemical and Process Engineering, University of Leeds, Leeds, LS2 9JT

3 Department of Mechanical Engineering, University of Sheffield. Mappin Street, S13JD, Sheffield

Abstract

Combustion of individual particles of different woody and agricultural residue biomass have been studied under a laboratory scale rapid-heating apparatus. Particles used were in the size range of 300- 1400 mm and weight 0.5-7 mg. A wire mesh element is used to radiatively heat the particle to 1200-1400K. The apparatus allows a high-speed camera to record the combustion of the individual particles directly. Examination of the resulting video images showed a sequential combustion of volatile matter followed by burn-out of the remaining char for all fuels. Analysis identified differences and patterns in burnout time, combustion behavior and the evolution of char size and shape transformations.

Heterogeneous behavior was observed between the different biomass samples and also among particles within some of the samples. Particles with initial prolate (fibrous) shapes have been observed to become more equant (quasi-spherical) during combustion. Measurement of the particle dimensions during its combustion extracted from the images of the high speed recording have allowed evaluation of the size and shape changes to be mapped. Particle size and shape appears to change only slightly during devolatilization and swelling was rarely observed. Following devolatilization, during the remaining char combustion, more pronounced

31 changes in the size and shape of the particle are apparent. In most cases the shrinking char

32 becomes more rounded as the char particle partially melts and contracts due to surface tension.

33 This transformation is more distinct in some of the biomass samples. Profiles and images of

34 the different fuels examined are presented.

35

36 Keywords: combustion, biomass, char shape

37 *Corresponding author:*
38 e-mail: hannah.chalmers@ed.ac.uk
39 Tel: +44 (0)131 6507444, fax. +44 (0) 1316506554

40

41

42 HIGHLIGHTS

43 • Combustion of single particle of five different biomass fuels

44 • Thermal imaging camera was used during combustion

45 • Biomass char shape and aspect ratio was calculated during combustion.

46 • During char combustion, particle shape changes from elongated (prolate) to spheroid

47 (equant) are observed

1. Introduction

Biomass power plants can provide large scale reliable energy with the flexibility to meet potentially unpredictable electricity demand. Biomass power is classed as a renewable source and is a key option for achieving a low-carbon electricity supply while meeting environmental targets on emissions and renewable energy. Many different biomass sources have been studied as fuels with a wide range of physical and chemical properties. The standardization of biomass fuel in the form of high energy-density pellets allows easier management and more sustainable transport to all scales consumers [1]. This also facilitates reliable performance of combustion plant with less variable ash content and calorific value of the fuel. Large power plants such as Drax and Lynemouth in the UK have opted for high quality biomass pellets to minimize problems in the combustion process. However this high standard on biomass fuel quality makes it also more expensive. A more diverse range of source materials will benefit with lower prices. However, lower quality fuels present technological challenges for biomass power plants in maintaining combustion efficiency, avoiding ash fouling issues and complying with strict pollutant emissions limits. Overcoming these challenges will enable better use of limited biomass resources such as new biomass fuels, from energy crops and residues.

Single particle combustion (SPC) devices are relatively simple experimental apparatus that can provide reliable information to study the main variables that affect combustion kinetics and compare different fuels combustion behaviour [2, 3, 4, 5, 6]. Biomass has high volatile matter content, less carbon, more oxygen and a lower heating value than coal. Moreover, due to higher reactivity of biomass, a bigger particle size range can generally be used for biomass fuels compared with pulverized coal. Previous studies on single particle device, provided an approximation to milling requirements for biomass fuels in terms of maximum particle size for efficient burn-out [7, 8]. Other single particle studies have identified the differences between different fuels behaviour during combustion [7, 3, 8, 9], providing details on ignition [10, 11,

73　12, 13], volatile flame [14], char combustion [15], particle morphology [16], combustion

74　atmosphere [17,18] or temperature [8, 18]. Flower et al. [5] conducted biomass single particles

75　studies in a wire mesh single particle setup for particles between 5 and 30 mg and showed

76　relatively low dependency on the aspect ratio of the samples. Mason et al. [3] performed a

77　series of single particle experiments which identified useful empirical functions to describe the

78　relationship between particle size and burnout time, allowing the behaviour of different fuels

79　in a furnace to be compared.

80　Biomass shows significant differences in ignition and combustion temperatures and burnout

81　times [2]. The observations made on small scale lab combustion produce relevant information

82　on the combustion behaviour for comparison among different fuels. This information together

83　with other parameters can be used for computer fluid dynamics (CFD) modelling of the

84　combustion process at any scale. CFD has been increasingly improving the resolution of the

85　combustion process modelling in recent years, providing better prediction results for new

86　developments. This has enabled lower pollutant emissions such as NO_x reduction [19] to be

87　achieved through optimised process design.

88

89　The shape, size and density of the particle is important for fluid dynamic modeling as it can

90　affect the trajectory and residence time of the fuel particle inside the boiler [20]. Large particle

91　size implies ignition delay [21] and longer burnout time [3,7], and therefore higher amount of

92　carbon in ash in a furnace. The monitoring and control of fuel particle size distribution is

93　important to achieve a complete and efficient combustion. Panahi et al [21] reported on recent

94　studies the spheroidation of elongated biomass particles with an initial aspect ratio between 4

95　and 8 becoming almost spherical during pyrolysis. This spheroidation is explained because

96　measured temperatures during volatile mater combustion are higher than the melting point of

97　main biomass components as cellulose (732- 739 K). They also concluded higher aspect ratio

98   leads to faster ignition. Bonefacic et al [20] analyzed the influence of the geometry of particles

99   in the combustion process. Their model revealed that particle geometry has a significant impact

100   on the starting point and the rate of devolatilisation as well as the char burning. Higher aspect

101   ratio of the particles leads to increased scattering of fuel, accelerating the devolatilization

102   process and enhancing the mixing of volatiles with the air. Yang et al. [22] developed a

103   mathematical model that predicts the behavior of a range of particles of different sizes,

104   demonstrating the occurrence of the general features of combustion and the occurrence of a

105   combustion wave. It explained the differences observed between spherical and cylindrical

106   biomass particles. These observations are consistent with experimental observations made by

107   same authors using suspended biomass particles and other works in the literature. Gubba et al

108   [23] validated a CFD model including different particles shape distribution and found

109   significant influence of the internal thermal gradients on the surface temperature, residence

110   time and combustion performance. Momeni et al [24] also studied shapes and size effect on

111   combustion process of single biomass particles, cylindrical particles were found to lose mass

112   faster than spherical particles and the burnout time was shortened by increasing the particle

113   aspect ratio (surface area). Similarly, Lu et al [25] obtained differences during devolatilization

114   depending on the shape of the initial particle. The conversion times of cylindrical particles with

115   almost the same surface area/volume ratio are very close to each other.

116   It is clear from the literature, that assuming that fuel particles are approximately spherical is a

117   reasonable approach for modeling some solid fuels like coal, obtaining good agreement with

118   experimental results [26, 27]. However this assumption is generally not enough for

119   lignocellulosic biomass which tends to have elongated particle shapes. The model developed

120   by Yang et al. [22] predicts a change on particle shape. However more detailed experimental

121   data in the literature on the evolution of particle size, shape, or temperature changes during

122   combustion of different biomass fuels is needed.

123

124   Combustion experiments on a single particle combustion apparatus have been undertaken using

125 various biomass materials with the objective of evaluating the differences among particles of

126 different biomass fuels on their combustion; including volatile burning time, char combustion

127 time, particle temperature and adding new information regarding particle size and shape

128 changes. The dimensions of the particle during combustion have been measured providing

129 precise novel data regarding shape and size changes during combustion of different biomass

130 materials. The study examined a range of biomass and different particle sizes compare times

131 required for burnout for the different fuels. The information provided by the video observation

132 can also provide fundamental data for other researchers developing new models to more

133 accurately describe the changes in particle size and shape during combustion process at a

134 particle level.

135

136 **2. Materials and methodology**

137   **2.1. Fuel samples used**

138   A series of experiments have been made with five different biomass samples. The biomass

139 sample used were pine (PI), eucalyptyus (EU), willow (WI), olive waste (OW) and steam

140 exploded wood ('black') pellet (BP). Each fuel was characterized in terms of chemical

141 composition by proximate analysis, ultimate analysis, and gross calorific value. Results are

142 presented in Table 1.

143   **Table 1. Proximate and ultimate analysis of the samples used.**

		Pine	Eucalyptus	Willow	Olive residue	Black pellet	Basis	units
Proximate Analysis	moisture content	8.3	8.1	3.1	5.9	7.2	as received	%wt
	ash content	2	0.9	2	7.6	4.2	d.b.	%wt
	volatile content	80.85	82.55	81.93	74.01	76.07	d.b.	%wt
	fixed carbon	17.15	16,55	16.07	18.39	19.73	d.b.	%wt

GCV (dry)		18.6	19.4	19.8	20.1	20.0	d.b.	MJ.kg^{-1}
Particle density		0.48	0.67	0.52	1.3	1.26	d.b.	mg.mm^{-3}
Elemental Analysis	**C**	46.45	48.76	49.78	48.79	50.49	d.b.	%wt
	H	5.19	5.55	5.88	6.01	5.56	d.b.	%wt
	O	44.98	44.69	41.85	36.13	39.47	d.b.	%wt
	N	1.27	0.1	0.39	1.48	0.19	d.b.	%wt

144

145   Each sample was milled, dried and sieved to obtain different ranges of sizes

146   The particle size ranges used for the experiments were 300--1400 μm. These sizes were

147   selected to be high enough to have meaningful images for the shape analysis and targeting with

148   the thermal imaging camera while being small enough to enable the assumption of uniform

149   particle temperature (i.e. thermally thin). This upper range is also representative of the largest

150   size fraction that would typically be used in a pulverized fuel boiler. Samples were dried in an

151   oven at 115 ºC for 2 hours to remove any moisture before combustion experiments in the wire

152   mesh reactor.

153

154   **2.2. Experimental device**

155   The experimental device used at the University of Edinburgh has been previously described at

156   [7]. The wire mesh reactor (WMR) apparatus used in this work allows a stationary particle

157   sample to be recorded with high speed video camera as it burns. The reactor was based on the

158   WMR used by Flower et al. [5], and is shown schematically in Figure 1. The particle under test

159   is supported between 2 vertical wire meshes that heat the particle by radiation, which is

160   consistent and permits reproducible results. The electrical current through the elements can

161   heat them to their operating temperature within 500 ms, which is small compared to particle

162   burning times. The output current was limited to enable an operating mesh temperature of 900

163   ºC, and estimated heating rate of ~10^3 ºC s-1. The reactor temperature was measured with an

164   k-Type thermocouple centred between the two meshes to ensure that the heat flux was

165   consistent between runs, permitting valid particle-to-particle comparisons. The sample holder

166 was placed on the centre line between the meshes The sample holder was made of the same

167 wire mesh material as the heating elements, forming a rectangle of 3 x 6 mm to place the sample

168 over it. The effect of mesh heating rate and final temperature affects the particle ignition delay,

169 but once the particle ignites the heat coming from the combustion becomes the main source of

170 energy for the particle temperature. Small errors on the mesh temperature will, therefore, have

171 little effect during the combustion performance and burnout time.

172 The high speed camera used in this study was a Phantom Miro eX4 with a zoom lens coupled

173 to a 20 mm expansion tube to give image magnification. It was placed on the top of the

174 apparatus. The camera-to-particle distance was fixed so that a consistent optical magnification

175 was achieved. The high speed video recording allowed a good temporal resolution to be

176 achieved. 500 frames per second were normally used for the recording exposure time of 3300

177 µs and resolution 128X128 pixels. A PC was used to retrieve the images from the camera and

178 all the videos were analysed using Phantom Control Camera. The recording was played back

179 in real time and at reduced speed, allowing observation of much smaller particles and also

180 phenomena that would be missed with a normal camera. The times for the respective phases in

181 particle combustion were then accurately determined by processing the video image files and

182 representative rankings of burning times were obtained. All particles were weighed before the

183 experiment and the burnout time for each particle could be measured from observation of the

184 video.

185
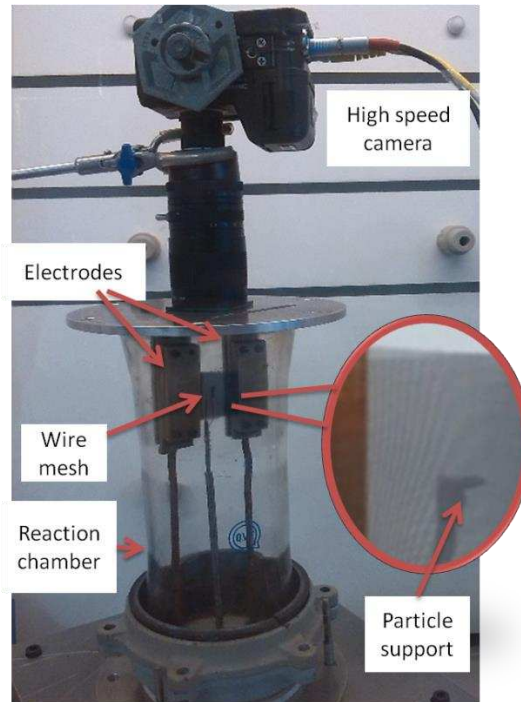
Figure 1. Single particle experimental setup.

187

2.3. Thermographic imaging

Measurement of the surface temperature of the combusting particle was possible by use of thermal imaging. In this study, a FLIR A600 series infra-red thermographic camera was used for this purpose. This camera has a focal-plane-array thermal detector with a measurement range up to 2273K and sensitivity specified as 0.05K with an accuracy tolerance of 2% of reading (i.e. ±30K at 1500K).

The images are derived from the intensity of the infra-red radiation detected by the thermal detector in the camera. The temperature of the particle's surface can be derived from the data although it is necessary to account for the emissivity of the surface. An emissivity of 0.85 was adopted for the entire range of the combustion process being observed with thermal imaging based on reported values for biomass char [28]

199

3. Results and discussion

3.1. Ignition and combustion behaviour analysis

All biomass fuels studied presented a sequential combustion with two well differentiated stages, volatile flame and char combustion. This is in agreement with previous works completed with this, and other single particle devices [2,3,4,7]. Upon ignition, the gases released through the pores of the particle created a smooth volatile flame surrounding the particle. This volatile flame became bigger and increasingly luminous and then shrinks to extinction. Char ignition follows until completion of particle char burnout. Figure 2 shows images from the videos of all biomass samples examined at different stages of combustion. Video files can be found on supplementary material section. In order to measure the burnout times and compare between the different tests, 0% burnout is the last frame before visible ignition takes place and 100% the first frame where there is not any visible combustion at all. The brightness and contrast of the images at 0% burnout were adjusted in order to have a clearer image of the original particle. It is noted that OW was especially difficult to distinguish from the background support so the particle perimeter is underlined in blue in the first image.

3.1.1. Ignition delay

The delay between the start of heating to particle ignition is very consistent between the different runs and different samples. However the delay can increase significantly with higher moisture content, as observed by previous studies [3].

3.1.2. Devolatilisation

After heating and drying, the pyrolysis reactions start to take place and they continue until a stable char is formed. In fast pyrolysis, biomass decomposes very quickly generating mostly gas, vapours, aerosols and char. The biomass pyrolysis starts releasing light hydrocarbons and main products such as H_2, H_2O, CO, CO_2, and CH_4. These products start the ignition of the volatile flame. The biomass particles appeared to start releasing volatiles a few milliseconds before ignition, this was visible on the images of the olive waste which produced a blurry image

226 and darkening on the surroundings of the particle. Nevertheless, the ignition delay time is

227 negligible in respect to the overall burnout time.

228 All samples showed homogeneous ignition and no significant differences were observed in

229 the volatile flame development. As the temperature increases, biomass fuels decompose into

230 primary volatiles. At temperatures above 773 K, the primary volatiles are subject to a secondary

231 pyrolysis, during which the tars are converted into a variety of gaseous species, especially CO,

232 light hydrocarbons, hydrogen and CO_2. The pores of the particle become open and connected

233 after a mass-loss front (moisture evaporation or devolatilisation) propagates from the particle

234 interior [22]. The gases from pyrolysis reactions flow through the porous medium inside the

235 particle reaching the surface and creating the volatile flame around the particle. As the pyrolysis

236 completes, the volatile flame shrinks as can be noted on the images for WI and PI comparing

237 25% and 45% burnout images on Figure 2. As the outward flow of pyrolysis products reduces,

238 the oxygen reaching the solid surface increases and char ignition is initiated.

239 There are notable differences between the samples regarding the times required for volatile

240 burning. The composition of biomass, the amount of volatiles and the pyrolysis kinetics of each

241 biomass, affects the duration of the volatile flame. Average volatile/char burning percentages

242 are presented in Figure 4. As shown on Figure 2, at 25% the video shows the volatile flame

243 surrounding the contour of the biomass particle very clearly in the case of EU, PI and WI. In

244 the case of BP the particle is in transition to char ignition, while the OW particle shown in the

245 figure has already completed the volatile combustion stage and the remaining char particle has

246 ignited at one end of the particle.

247 The EU particles had the most elongated shaped particles. Given that, it was observed that

248 the volatile flame in the centre of the particle and char ignition on both ends of the particle

249 overlapped for a few milliseconds. On the contrary, BP sometimes exhibited a few milliseconds

250 delay between the volatile flame extinction and the complete ignition of the char. This is not

251 the case on the BP particle on Figure 2 at 25% where there is still some blurriness due to the

252 end of the volatile flame while the char particle on the background has already ignited.

253   WI and PI continue showing volatile flame at 45% burnout, and even at 60% burnout the

254 WI particle shows a small volatile flame while the char has completely ignited.

255
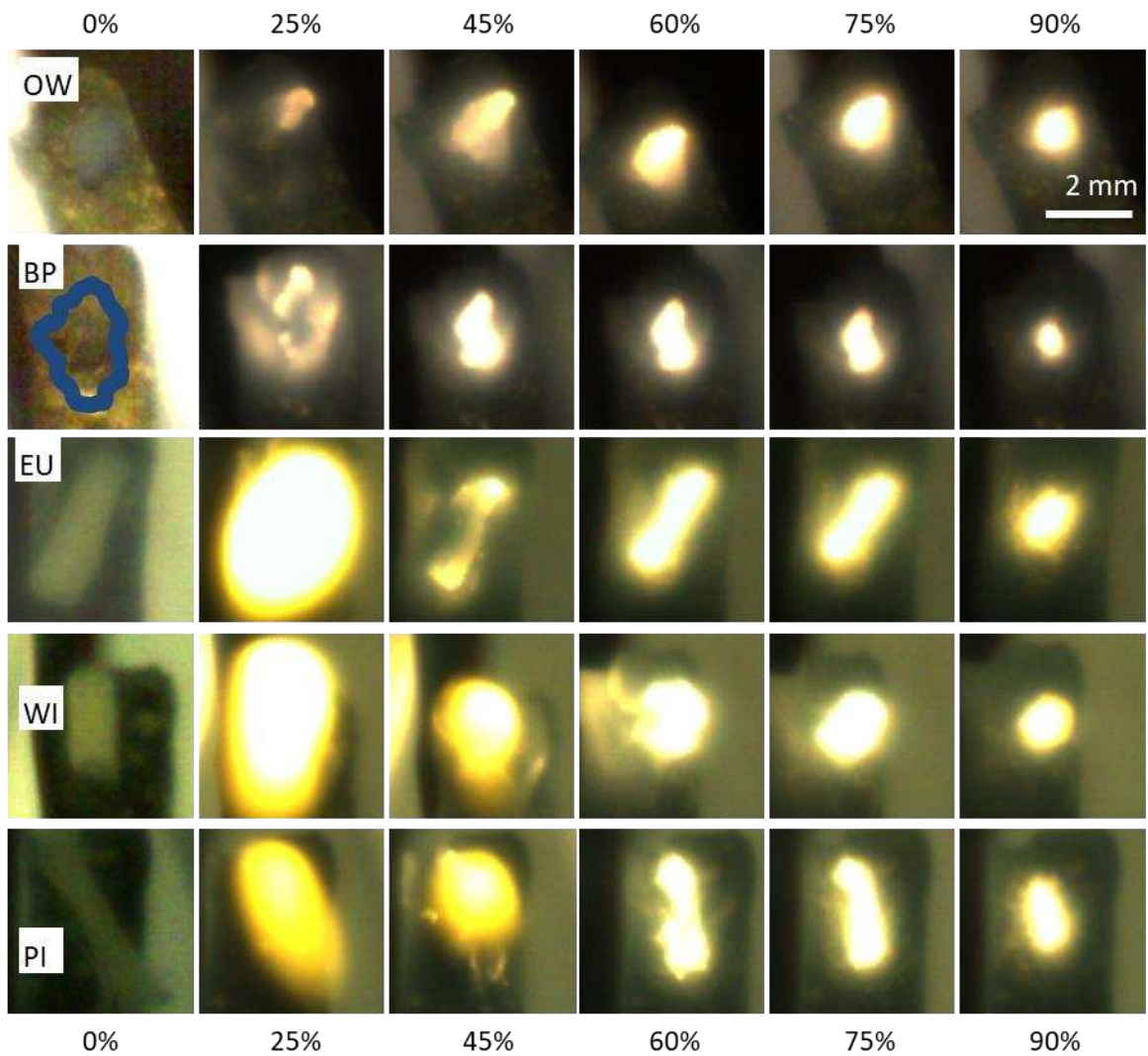
Figure 2. Images from the combustion recording of: olive waste (OW) steam torrefacted wood pellet (BP), eucalyptyus (EU), willow (WI) and pine (PI) particles at different percentages of burnout time.

259

3.1.3. Char combustion

261   For some cases the flame front could be observed during particle char ignition. Comparing

262   OW particle at 0% and 45% burnout in Figure 2, it can be observed that the particle moved or

263   changed during the devolatilization stage. In this particular case, the particle just rolled over

264   the support. Changes were occasionally observed with deformations and bending of some

265   particles. Swelling has also been observed in some cases; however there was not a significant

266   number of swelling cases at the volatile burning stage for any of the samples tested to quantify

267   this. The majority of them remain unchanged or shrink slightly on the major axis (length). An

268   increment in the size of the particle was observed on the minor axis (width) in some particles

269   during devolatilization. Rather than swelling, as some bituminous coals do, this phenomenon

270   can be attributed to the separation of fibres of the particle. Images from the char at the different

271   stages of combustion evidenced particle shape changes. The observartions of particle shape

272   and projected area evolution observations are addressed in detail in section 3.4.

273   At the end of the particle combustion the ash remains incandescent over the support for a

274   few milliseconds before cooling down. It is observed that the ash distributed all over the particle

275   is transported during char combustion. While the particle is consumed the ash reaches the

276   particle surface. In some of the particles, the ash creates a coarse surrounding the particle. At

277   100% burnout, the coarse ash remains incandescent with a shape that is proportional to the char

278   particle on its last stage of combustion.

279

280   **3.2. Burnout time for single particle combustion**

281   Particles of different weight and sizes were evaluated through the single particle

282   experimental device in order to study the effect of particle size on the combustion behavior of

283   the fuels as well as their burnout time. The variability on the aspect ratio of the woody biomass

284   particles makes the relationship between particle cut size and particle mass imprecise. As a

285   result, it is difficult to predict accurately a biomass particle mass for a given particle cut size.

286   Therefore this relationship needs to be taken with its limitations and results are represented

287   based on particle weight not on their size. The corresponding range size will depend on

288   roundness of each fuel particle. A significant number of experiments were done with each

289   sample on a range of weight from 0.5mg to 5 mg. Some experiments were done with particles

290   above 5 mg in order to ensure the trends obtained are in agreement with previous results [3, 5,

291   7] The particle weight versus burnout time for each particle of the different biomass tried is

292   plotted in Figure 3. The deviation of the trend is large for some of the particles also because

293   the heterogeneity of biomass particles composition.
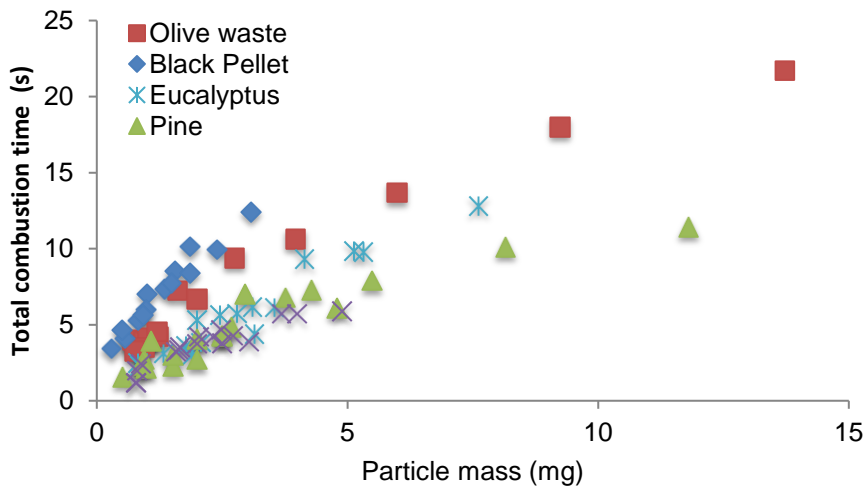
294

295   **Figure 3. Burnout time obtained for different biomass samples**

296   The burnout time increase with the increment of particle weight for all samples. The

297   relationship between weight and burnout time results for biomass particles were consistent with

298   that observed in previous SPC studies [3] where the data could be fitted to a regression function

299   of the form t=a.mass^b where a and b are empirically derived coefficients. In this study, the best

300   adjustments were obtained for a second order polynomial function. Equations and R^2 values

301   are represented on Table 2. The burnout time trend lines versus particle mass cannot be directly

302   transposed to large scale conditions burnout times, as the heat transfer and combustion

303   conditions are different, but it provides a useful means to compare different biomass samples.

304 For a better comparison among the samples, values for extrapolated burnout time for volatiles

305 and char for a particle of 2 mg are plotted on Figure 4.

306

307 **Table 2. Burnout time, normalized projected area and char temperature observed for the**

308 **different samples**

Sample	Burnout time	R2	Range	Char Temperature	Normalized Particle Projected Area	R2
BP	$t = -0.384m^2 + 4.454m + 2.11$	0.959	0.5 - 3 mg	-	$A = -79.93t^2 + 5.565t + 100$	0.965
OW	$t = -0.428m^2 + 4.34m + 0.25$	0.951	0.5 - 4 mg	-	$A = -169.49t^3 + 83.997t^2 + 19.314t + 100$	0.9864
EU	$t = -0.028m^2 + 1.857m + 0.59$	0.935	1 -7 mg	1405	$A = -88.83t2 + 8.6t + 100$	0.959
PI	$t = -0.075m^2 + 1.787m + 0.64$	0.979	0.5 - 5.5 mg	1422	$A = -271t^3 + 319t^2 - 123t + 100$	0.9593
WI	$t = -0.246m^2 + 2.43m - 0.11$	0.943	1 -5 mg	1392	$A = -115.6t^2 + 55.5t + 100$	0.981

309

310 The differences observed between samples must be attributed to the differences on reactivity

311 of the fuels. The regression functions for WI, EU and PI were almost overlapping. WI was

312 slightly lower, which suggests a higher reactivity, being therefore the most reactive of all

313 samples tried. OW was notably above those. Olive waste is been reported in the literature to

314 have lower reactivity than other biomass due to high content in lignin [29, 30]. The steam-

315 exploded wood pellet (BP) sample showed the lowest reactivity with the longest burnout times.

316 The raw material before torrefaction was not available to compare in this study, so the low

317 reactivity cannot be attributed to the process of torrefaction alone. However, Jones et al [31]

318 reported that torrefaction produced less reactive biomass chars, similarly Vorobiev et al. [32]

319 reported that the char burnout rate was found to decrease with torrefaction intensity of beech

320 wood. Other works by Lu et al [33] did not find differences on intrinsic reactivity as determined

321 by thermogravimetric analysis due to the torrefaction pretreatment, but the torrefaction

322 increased char yield and char particle density.

323
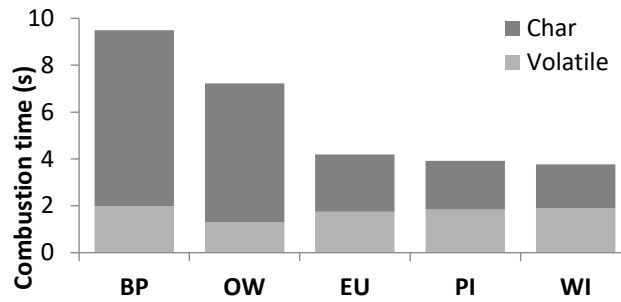
Figure 4. Average burnout time obtained for a 2 mg particle of the different biomass samples.

The average volatile/char time ratio remained constant along the range of particle sizes tried (1-5 mg) for all samples. For the biomass samples EU, PI and WI, the volatile pyrolisis and burnout time was practically equal to the char burnout time. These three samples showed similar times for volatile burning, aligned with very little differences on volatile matter content from the proximate analysis. The volatiles combustion times account for 40 to 50 % over the total combustion time, which is clearly distinctive to OW and BP that account 18 to 20 % on average. This is partially correlated with volatile matter content obtained on the proximate analysis that ranges 80.8-82.5 %, as it can be seen on Figure 5. Olive waste shows a shorter volatile burnout time, as expected due to lower volatile matter content from proximate analysis (74%). Torrefied pellet has a 78% volatile matter on proximate analysis, however the burnout time is slightly higher than the higher volatile matter biomass but the main difference is on the char burnout time, that may be attributed to low fuel reactivity.

Particle density is significative higher on both OW and BP, this has a worsening effect on the heat transfer from the mesh to the particle that could also delay the pyrolysis and char combustion reaction.

The correlation between parameters from proximate analysis, such as volatile content or fixed carbon is not enough to predict burnout times for volatile matter or char combustion times, reflecting the complexity of combustion process on pyrolysis and combustion kinetics.
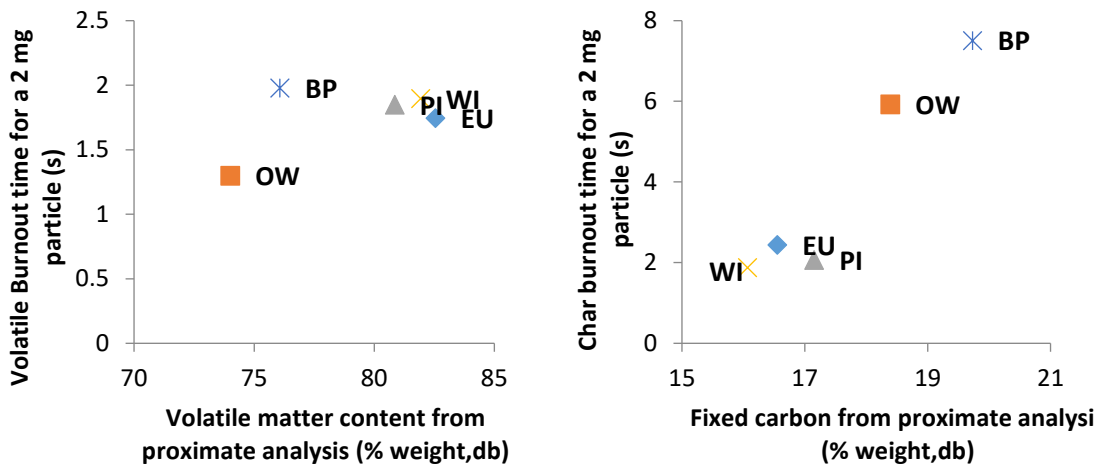
Figure 5. Burnout time for volatiles (a) and char (b) for a 2 mg particle of the different biomass samples versus volatile matter and fixed carbon from proximate analysis respectively.
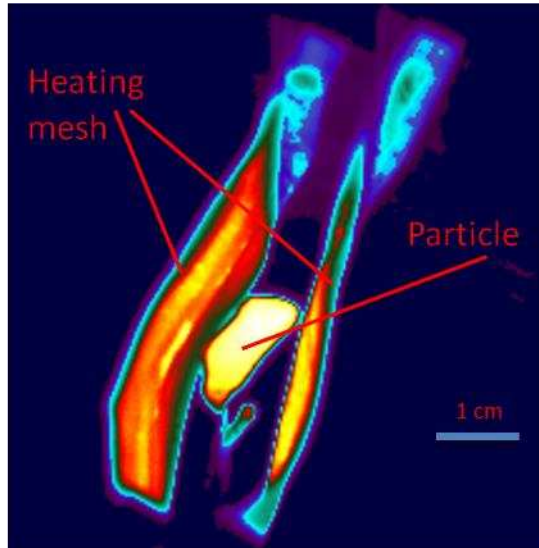
Particle size distribution and milling process is important for an efficient combustion of fuels. This is especially important on fuels with low reactivity. However for biomass with high reactivity, the burnout time exhibits a lower variation with particle weight or size. This would allow the fuel processing system to be more flexible on its outcome and have less milling energy requirements. In those cases, other parameters such as moisture could be as relevant as the particle size.

3.3. Thermal imaging

The single particle combustion experiment was performed also using a thermal imaging camera instead of the high-speed camera. The experiments were done for three of the samples: PI, EU, WI. Images were obtained through the entire combustion process for a number of particles of each sample. An example image is presented in figure 6. The surface temperature of the particles was subsequently extracted from the image data and the results are presented in figure 7.
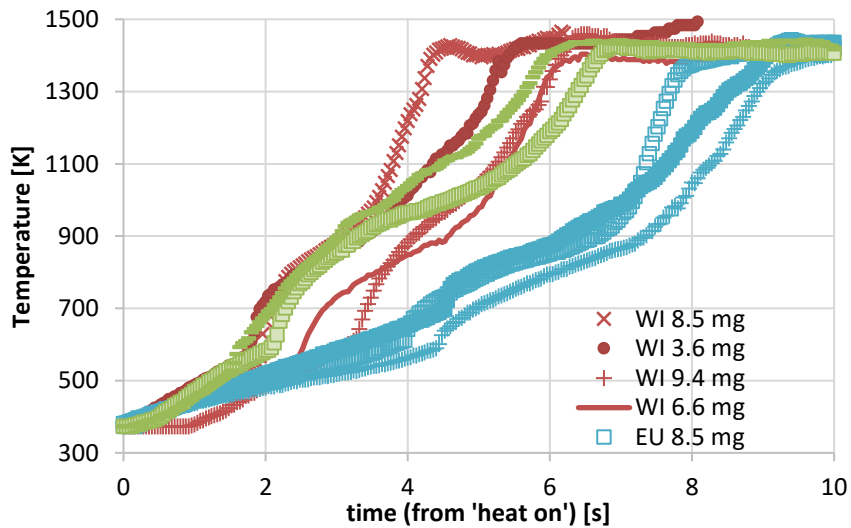
Figure 6 – Thermographic image of particle of EU biomass in wire-mesh reactor

Figure 7 . Surface temperature time-history profile of combusting particles of PI, WI

and EU derived from thermal imaging.

The surface temperature profile for a number of particles of PI, WI and EU samples is presented in Figure 4. After start heating, the particle surface temperature raises up relatively slow until volatile ignition. Two main increments of the heating rate are observed on the temperature-time profile, corresponding with two changes on slope trend. First notable

377 increment of the surface heating rate is observed when the volatiles ignite with surface

378 temperatures in the range of 500 to 600 K. Pine particles seem to develop a slower heating rate

379 on the surface of the particle. The surface temperature continues increasing on a slower heating

380 rate after volatile ignition. Second increase of the heating rate is related with char ignition, with

381 temperature raising fast until reaching a plateau at a temperature on the range of 1390- 1430

382 K. Average plateau temperatures for the three samples tested are listed in Table 2. No

383 significative differences were observed among the biomass samples on the plateau temperature

384 during char combustion.

385

386 **3.4. Shape change during particle combustion**

387 No regular behaviour was detected for all particles on their shape and size evolution during

388 combustion. Despite similar origin, shape, size and conditions, different behaviors were

389 observed on the particles of each fuel. In some aspects, even opposite trends were observed as,

390 for example, some particles swell and some shrink at the pyrolysis stage.

391 Length and width dimensions of the particle where recorded at different stages of combustion.

392 A proportional decrease of the particle size would be initially expected during the char

393 combustion. However, this is not what was observed for these samples. As the char combustion

394 progresses the particles instead become more rounded. The shape of the particles with higher

395 aspect ratios changes from a fibrous shape to an ellipsoid that appears to be consumed only in

396 the direction of the length. During volatile flame combustion the particle was not visible at all

397 due to flame screening, however measurements on particle size before ignition and during char

398 combustion where relatively straightforward to take from the video frames. In order to facilitate

399 the comparison among the particles and samples, combustion time, normalized to 100% of total

400 burnout time, for each particle was used. The aspect ratio defined as the length divided by width

401 was also calculated at the different stages of combustion. Some particles were observed to bend

19

over themselves and therefore had to be discarded for the aspect ratio analysis. Some particles

were cut manually so the initial dimensions do not necessarily represent the dimensions coming

from an industrial mill. The aspect ratio however is on the range of values that would be

expected on a large scale milling. Initial aspect ratio for EU, PI and WI were higher than BP

and much higher than OW.

The sample of pine biomass (PI) used had the largest aspect ratio of the samples tried with an

initial value of 5.96. No swelling was observed on the vast majority of PI particles. After

devolatilization most of the particles shrink slightly on their length, keeping normally the same

width as the initial particle. So the aspect ratio of the char obtained after devolatilization was

close to the size of the initial particle or slightly lower. During the char combustion stage, the

particles are consumed mainly on the tips, while the observed width of the particle remains on

similar values as the initial particle until well advanced burnout times. Therefore the aspect

ratio of the particle reduces due to length reduction of the burning char. Figure 8 represents the

average observed aspect ratio of PI particles as well as the standard deviation versus the

normalized burnout time.
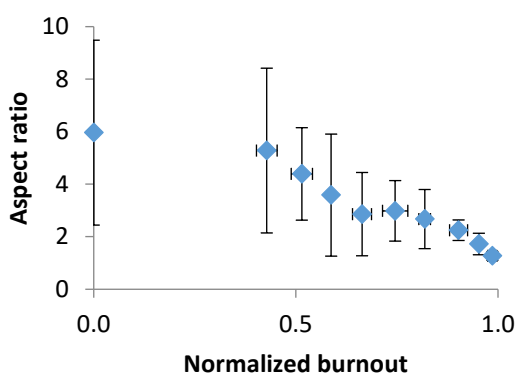
Figure 8. Evolution of the average aspect ratio during combustion of PI particles.

421 EU particles had an initial aspect ratio of 4.7, large differences are observed between length

422 and width. A few representative particles of the evolution of the dimensions of EU particles

423 are represented on Figure 9 (length) and Figure 10 (width). On the length the particles observed

424 gradually decrease on size, the dimension evolution on the largest size of the particle generally

425 trend to an asymptotic tendency towards a value around the width.

426
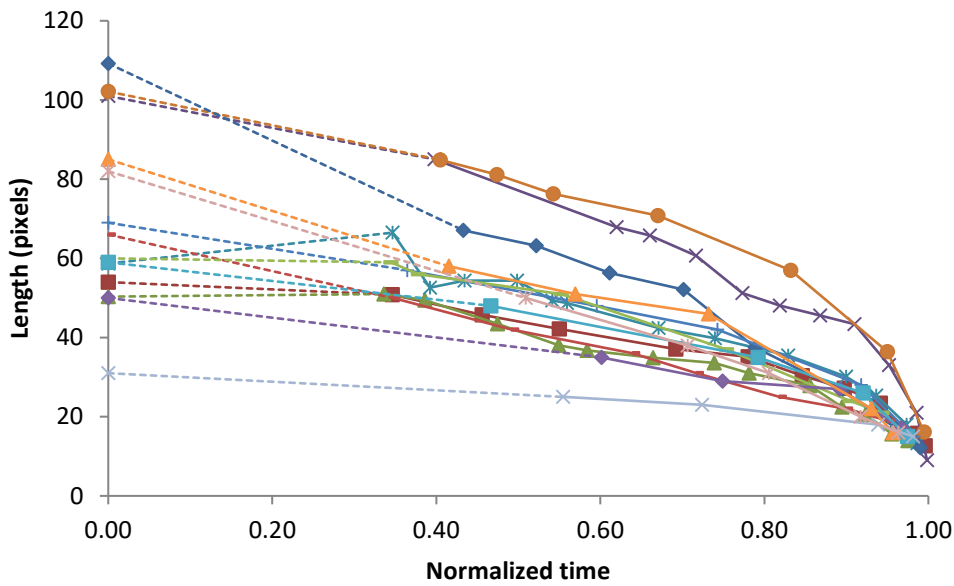
Figure 9. Evolution of the length measurements during combustion for various EU
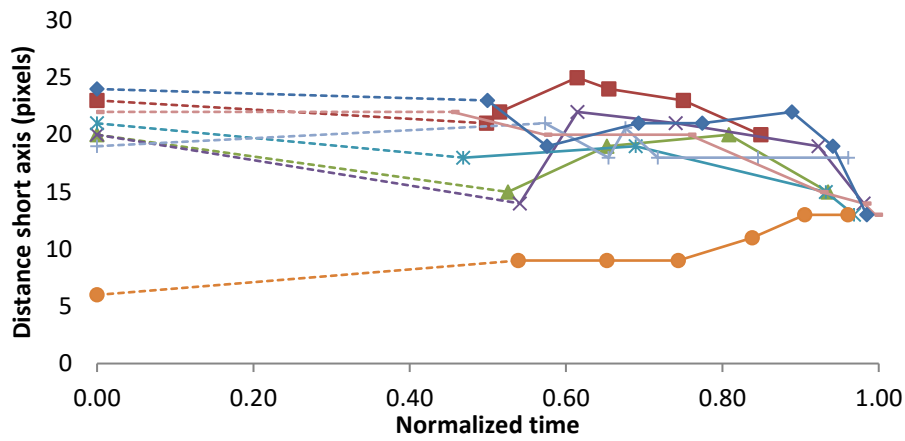
particles.

429

430
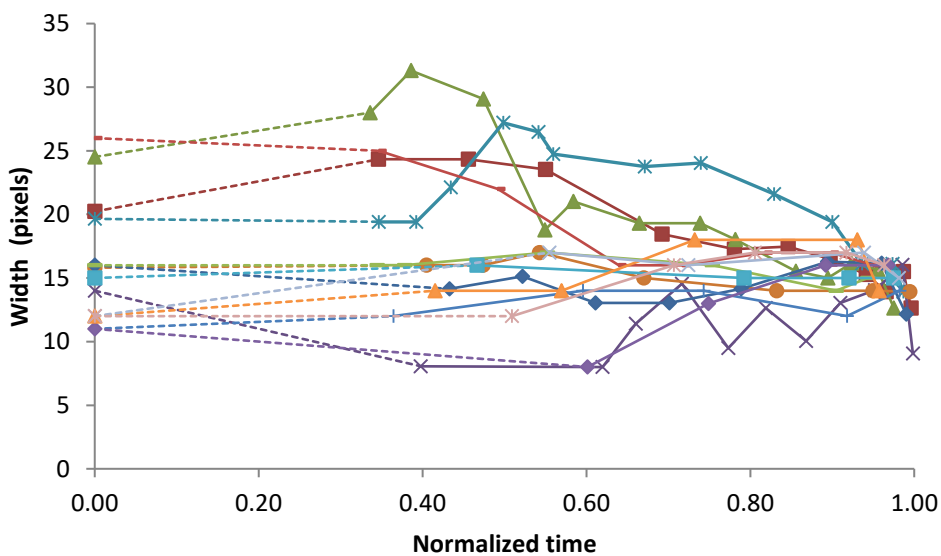
Figure 10. Evolution of the width measurements during combustion for various EU particles.

Diverse behavior is observed on the width, some particles present apparent swelling while others remain constant or decrease slightly. Those particles that swell during the first step of volatile release, decrease shortly after the ignition of the char surface. The swelling of the particle create a rapid enlargement of the particle dimension. The surface area and higher particle volume created reduces the density considerably. Therefore, once ignited, the char surface is rapidly consumed by the combustion reactions, which explains the fast change on the width on the particles that swell during the volatile combustion. Some particles showed swelling during different stages of combustion. Some particles showed swelling during the first stages of char burning. This could be associated with a higher temperature of the particle during char combustion compared to volatile combustion stage [8] and therefore a softening of the particle while pyrolysis reactions continue occurring inside the particle during char combustion. Particles presenting swelling are generally observed to have slightly shorter burnout time than the average.

WI particles did not show significant swelling. The particles shrink gradually on their length on the second half of the char combustion. As observed in the videos, the particle dimension on the width remains constant during the combustion until very end of the combustion (over 95% burnout).
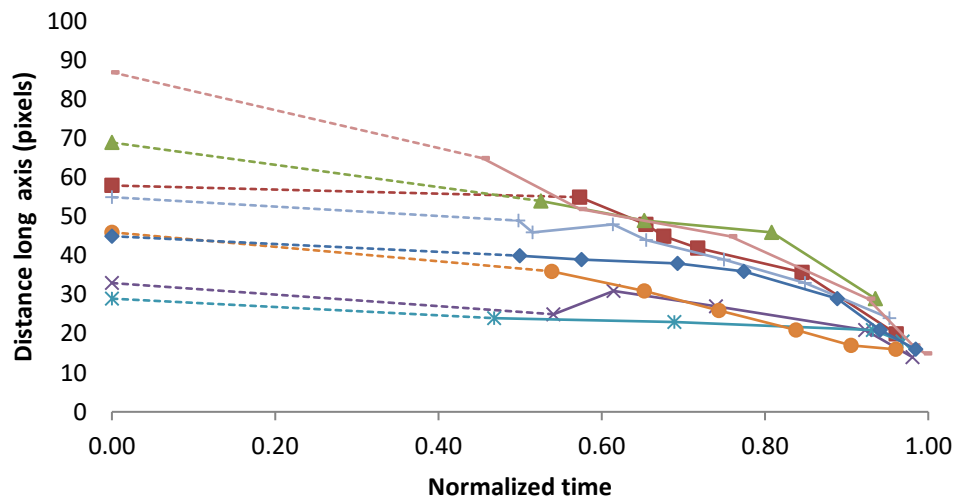
452

Figure 11. Evolution of the width measurements during combustion of various WI particles.

453
454

455

456

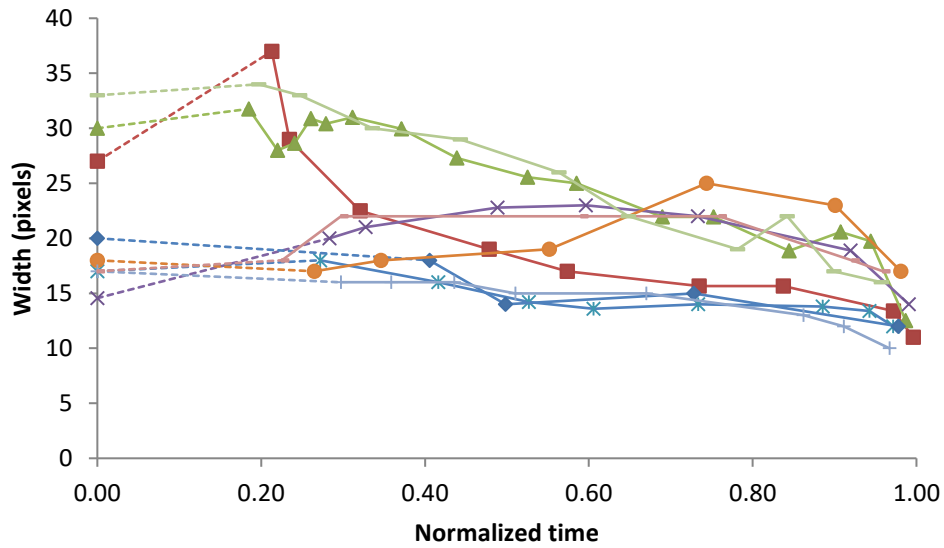**Figure 12. Evolution of the length measurements during combustion of various WI particles.**

457
458

459

Neither WI nor PI samples showed any swelling. A slight decrease in the length was observed on the willow particles after devolatilization stage that on average takes half of the total burnout time. No evidence was seen for particle shape changes during the volatile combustion stage for willow sample.

460
461
462
463

464 It is notable that particle width remains practically constant during combustion, even increasing

465 in some particles. This increase does not fit on the trend of a swelling particle, and is more

466 likely due to partial melting and spherification process. This was observed by Panahi et al. [21],

467 where much longer and thinner particles were observed to fuse and bend over themselves

468 leading to a almost round char. The different initial aspect ratio on the samples tried in this

469 study and [21] indicates that thin and long particles seem to have higher propensity to

470 spherification during the pyrolysis stage, although this process is not observed for all samples.

471

472 The olive waste has been extensively pressed in order to extract the oil so the raw particles are

473 quite round with initial aspect ratio of 1.3±0.36. Differences on the dimensions of width and

474 length were small. The size of the particle is reduced during combustion, however it doesn´t

475 decrease proportionally during time. Particles remain on proportionally large until almost the

476 end of the combustion. At 90% of the combustion time, some particles remain with similar

477 volumes, while some have been reduced to half and others are even larger due to particle

478 swelling. The volatile flame stage is much shorter on the olive waste sample. It was noted that

479 some particles showed swelling during char combustion stage. As previously described for the

480 EU sample, a rapid swelling on the pyrolysis stage is normally followed by a quicker

481 consumption of the particle and a large decrease in particle size shortly after the swelling. This

482 was also the case in a few OW particles, as represented in Figure 13. Both OW and BP present

483 a high particle density and more compact structure and much lower aspect ratio than the rest

484 of the samples. As described by Biagini et al [34], woody biomass samples present more

485 particles with a fibrous structure that is likely to shrink and fragment. While dense particles

486 with a compact structure are expected to experience minor variations in size

487

488 Particles presenting thin aspect do not decrease in size on the short edge size during

489 combustion. This observation was noted on all the samples studied. As observed in Figures 11

490 and 13, particles with initial small width, remain constant or decrease during combustion and

491 end with very similar width dimensions as the initial particle.

492

493 **Figure 13. Evolution of the width measurements during combustion of various OW**

494 **particles.**

495

496
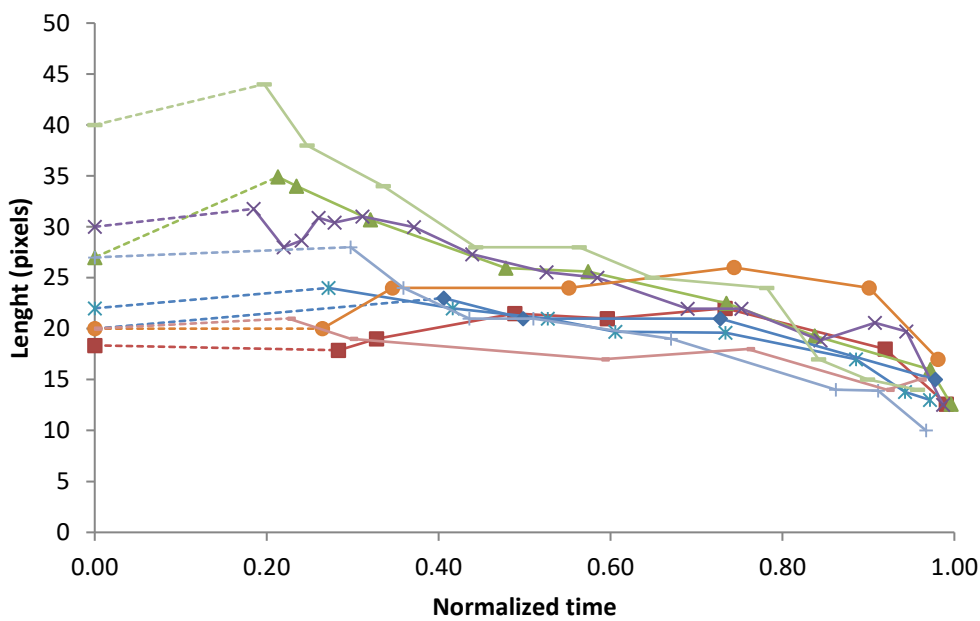
Figure 14. Evolution of the length measurements during combustion of various olive

498 **waste particles.**

499

500 Torrefaction tends to make biomass particles brittle [35]. So, during the processes of milling,

501 pelletization and pellet milling, the particles break, resulting in a lower aspect ratio than a non-

502 torrefied biomass fuel. The fuel sample from the steam-exploded wood pellets reflects this

503 brittleness with an initial average aspect ratio of 1.8, which is low for a woody biomass. The

504 aspect ratio evolution reflects a tendency for the particles to become more rounded at early

505 stages of char combustion. Figure 14 represents the average aspect ratio of the different samples

506 examined. During the volatiles combustion stage the particle was not completely visible and

507 the measurements could not be taken, so the linear evolution assumed during that time is

508 represented with dotted line.
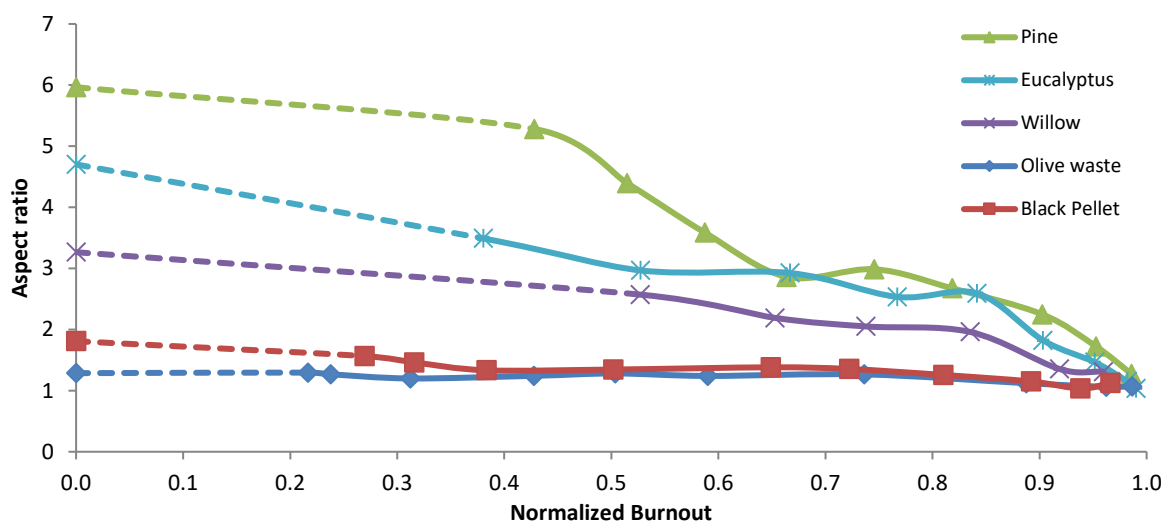
509

510 **Figure 15. Evolution of the average aspect ratio of all samples during combustion.**

511

512 Particle density is a key factor during combustion process. The samples with higher particle

513 density tried were OW and BP. These samples presented very small aspect ratios compared to

514 the rest of the samples, with close valued for width and length. The projected areas even

515 increase slightly during pyrolysis and sometimes during char combustion as well, as observed

26

average measurements on Figure 16. The char density has been previously reported to change

dramatically during combustion [30], not only due to pyrolysis but also due to the combustion

process on the char surface. The heterogeneous combustion reactions take place all over the

porous surface of the char and as progresses the oxygen reaches areas closer to the particle

centre. Thus the particle volume does not decrease proportionally to the combustion rate. As

observed from the projected area on the images, the particles with well advanced combustion

rates still have relatively large volumes. Projected area has been calculated assuming the

particles as ellipsoids, The equations for the projected area for normalized area of the different

samples are listed on Table 2, Regression lines of 2nd and 3th order polynomial have been

selected for best fit on each case according to R^2 values,
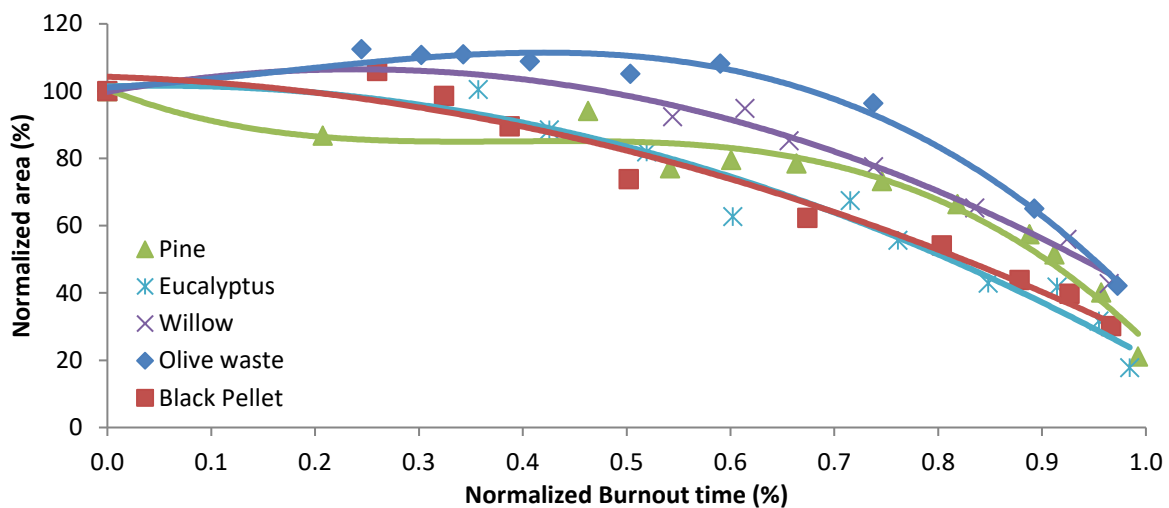
Figure 16. Evolution of the normalized projected area during combustion.

Li and Zang [36] developed a model for combustion of spherical particles that predicts the

particle shrinking during the char combustion. The model demonstrated that char consumption

is not uniform on the particle surface, being higher at the semi-major axis than at the semi-

minor axis. This leads to a decrease in the ellipsoidal particle size. The shape of the particle

has been also modelled in previous works, such as Yang et al [22], this works describe with

detail a model for a single particle combustion comparing shapes such as sphere and cylinder.

535   The combustion rate on the tip of the cylinder shape is predicted to be higher due to the thinner

536   boundary layer of the reactions front wave. Gradually the particle is assumed to become more

537   round due to higher combustion rate on the thermally thinner parts of the particle. The

538   observations on the particle shape from the videos of the combustion experiments presented in

539   this study do not match with a regular shrinkage. The changes on the shape cannot be only

540   attributed to a higher combustion rate on the tips of elongated particles. This is due to two main

541   observations: first, some particles preserve or even enlarge their width during combustion;

542   secondly the length of the particle shrinks on an irregular rate, accelerating by the end of

543   combustion. This second observation can be attributed to the progressive reduction of the

544   density of the particle. As the biomass char mass is consumed in the combustion process it

545   becomes lighter. The projected area does not reflect a linear reduction during combustion time.

546   As the width of the particles remains practically constant until the end of combustion, the

547   projected area is directly linked with the length of the particle. This relation is stronger for more

548   elongated particles. At the end of the combustion, with 90% burnout the particles are generally

549   equant in width and length. This observation is in agreement with other works such as [37],

550   where the wood particles were observed to change shape looking like droplets at the end of

551   pyrolysis at 1573 K on a drop tube reactor.

552   The projected area then remains circular and a final, very quick, reduction of the area is

553   observable after 90-95% burnout until the end. This has been previously observed by Levendis

554   et al. [38] and Khatami et al. [6] and is described as shrinking core combustion behavior by

555   Shan et al [39].

556   Particle temperature recorded with the thermal camera on the range of 1200-1400 K is enough

557   for melting of the main components of biomass (cellulose and hemicellulose). The melting is

558   likely to happen close to the surface, were combustion takes place and temperatures are high,

559   however the heat transfer between the surface and the centre of the particle is slower than the

560 combustion reaction and prevents the particle to become completely melted under the

561 conditions of this study. Mineral matter among the biomass can play a role in char softening

562 and shape changes, inorganic elements could be spread through the biomass material, and as

563 would be in the particles. Some elements such as Mg, P or K are present in higher concentration

564 in agricultural residues and can decrease the melting point of the ash due to eutectic melting

565 points. Proximate analysis on the different biomass shows high ash content on olive (7.2%),

566 and steam exploded pellet (3.9%) being low in willow and pine (1.8% both) and very low

567 (0.8%) in Eucalyptus. All of them showed shape transformation at different steps of the

568 combustion

569 The temperatures recorded during combustion can be enough to melt certain elements of the

570 ash by mid to end of combustion, as normally ash deformation temperatures for some biomass,

571 can start at 1200 k for biomass rich in K, being higher for those rich in Si or Ca. However the

572 main constituent will be organic material and therefore the main effect this inorganic elements

573 is the catalytic effect that can take part during pyrolysis. Some inorganic elements will catalyze

574 the pyrolysis reactions, accelerating the cracking reactions and allowing the char to get

575 plasticity at low temperatures.

576 Relatively low temperatures have been proven enough to part-melt biomass char compounds

577 as bituminous coals. Trubetskaya et al. [40] observed softening of the solid char matrix already

578 at 350 °C, being greater with increasing temperature and heating rate. This temperature is far

579 below the normal range of ash deformation temperatures. This can explain the slight increase

580 on the width of OR at early stages of the combustion, when temperatures are not expected to

581 be enough to melt main biomass initial constituents.

582 Some particles with prolate shape showed an irregular shape change in various stages. As it

583 can be observed in figure 15 for all samples and particularly for pine in figure 8, the aspect

584 ratio does not decrease following a linear regression. This can be explained due to the different

585 temperature on the out layer of the particle, allowing the particle to deform in the more exposed

586 areas

587 On a first stage the tips get rounded, decreasing the aspect ratio. However the inner structure

588 of the char at the center of the particle remains at lower temperature keeping the particle on an

589 ellipsoid shape until the combustion is well advanced. At the end of combustion, the

590 temperature gradient is negligible and the whole particle is at enough temperature to allow

591 plastic deformation to an almost spherical shape.

592 Surface tension of melted components of the char particle can play an important role on the

593 conformation of particle shape leading to a more rounded particle. This effect is stronger at the

594 end of combustion when particle has been heated for longer times and the combustion front

595 wave has reached the particle centre. Temperature gradient inside the particle will be then

596 negligible and high temperatures, close to the temperature measured on surface are expected at

597 the entire particle.

598

599 **4. Conclusions**

600 All samples presented homogeneous ignition and sequential burning of volatiles and char. BP

601 and OW had shorter volatile burning time, and longer char and total burnout times, .PI, EU,

602 WI were very close to each other with the half of total burnout time of BP. Temperatures

603 measured with the thermal imaging camera for PI, EU, WI show a plateau during char

604 combustion on the range of 1390-1430 K, with no significative differences among the samples.

605 The observed evolution of the dimensions of the particles differs from the gradually reduction

606 on size that would be initially expected. Little changes on the shape and size were observed

607 after the pyrolysis stage. Nor WI nor PI samples presented any swelling, while some particles

608 of OW presented slight swelling in some cases during pyrolysis or char combustion stages.

609 During char combustion the particles become more round. The shape of the particles with initial

610 fibrous shape, changes to an ellipsoid that apparently seems to be consumed only in the

611 direction of the major axis. During char combustion process, long fibrous particles reduce their

612 length, while the observed width of the particle remains on similar values as the initial particle

613 until well advanced burnout times. The projected area of the char particles with well advanced

614 combustion rates still have relatively large values. At the end of the combustion, with 90%

615 burnout the particles are generally equant in width and length. Partial melting of the particle

616 during char combustion allows the surface tension to modify the particle shape, leading to a

617 more round particle. The projected area then remains as a circle and finally a very quick

618 reduction of the area is observable after 90-95% burnout until the end.

619

626

627 **Supplementary material**

628 Video files are provided as supplementary material associated with this article and can be

629 found in the online version research data repository Mendeley Data.

630

631 **References**

632 [1] Ruiz D, San Miguel G, Corona B, López FR. LCA of a multifunctional bioenergy chain

633 based on pellet production. Fuel 2018; 215:601-611

634   [2] Riaza J, Ajmi M, Gibbins J, Chalmers H. Ignition and Combustion of Single Particles of

635   Coal and Biomass under O_2/CO_2 Atmospheres. Energy Procedia (2017), 114, pag. 6067

636   [3] Mason PE, Darvell LI, Jones JM, Pourkashanian M, Williams A. Single particle flame-

637   combustion studies on solid biomass fuels. Fuel 2015; 151:21.

638   [4] Marek E, Stańczyk K. Case studies investigating single coal particle ignition and

639   combustion. Journal of Sustainable Mining 2013;12:17.

640   [5] Flower M, Gibbins J. A radiant heating wire mesh single-particle biomass combustion

641   apparatus. Fuel (2009), 88, pag. 2418.

642   [6] Khatami R, Stivers C, Joshi K, Levendis Y, Sarofim F. Combustion behavior of single

643   particles from three different coal ranks and from sugar cane bagasse in O_2/N_2 and O_2/CO_2

644   atmospheres. Combust Flame (2012), 159, pag. 1253.

645   [7] Riaza J, Gibbins J, Chalmers H. Ignition and combustion of single particles of coal and

646   biomass. Fuel (2017), 202, pag. 650.

647   [8] Mock C, Lee H, Choi S, Manovic V. Combustion Behavior of Relatively Large

648   Pulverized Biomass Particles at Rapid Heating Rates. Energy and Fuels 2016;30:10809-10822

649   [8] Riaza J, Khatami R, Levendis YA, Álvarez L, Gil MV, Pevida C, et al. Combustion

650   of single biomass particles in air and in oxy-fuel conditions. Biomass Bioenergy 2014;64:162–

651   174.

652   [9] Shan L, Kong M, Bennet TD, Sarroza AC, Eastwick C, Sun D,Lu G, Yan Y, Liu H.

653   Studies on combustion behaviours of single biomass particles using a visualization method.

654   Biomass and Bioenergy 2018;109:54-60

655   [10] Carvalho A, Rabaçal M, Costa M, Alzueta MU, Abián M. Effects of potassium and

656   calcium on the early stages of combustion of single biomass particles.   Fuel

657   2017;209:787-794

658   [11] Simões G, Magalhães D, Rabaçal M, Costa M. Effect of gas temperature and oxygen

659   concentration on single particle ignition behavior of biomass fuels. Proceedings of the

660   Combustion Institute 2017;36:2235-2242

661   [12] Lu Z, Jian J, Arendt Jensen P, Wu H, Glarborg P.   Impact of KCl impregnation on

662   single particle combustion of wood and torrefied wood Fuel   2017;206:684-689

663   [13] Magalhães D, Kazanç F, Ferreira A, Rabaçal M, Costa M. Ignition behavior of Turkish

664   biomass and lignite fuels at low and high heating rates. Fuel 2017:207:154-164

665   [14] Lee H, Choi S. Volatile flame visualization of single pulverized fuel particles. Powder

666   Technology Volume 2018; 333: 353-363

667   [15] Schiemann M, Haarmann S, Vorobiev N. Char burning kinetics from imaging

668   pyrometry: Particle shape effects. Fuel 2014;134:53-62.

669   [16] Biagini E, Narducci P, Tognotti L. Size and structural characterization of lignin-

670   cellulosic fuels after the rapid devolatilization. Fuel 2008;87:177–186

671   [17] Lei K, Ye B, Cao J, Zhang R, Liu D. Combustion characteristics of single particles

672   from bituminous coal and pine sawdust in O2/N2, O2/CO2, and O2/H2O atmospheres.

673   Energies 2017;10:1695

674   [18] Riaza J, Khatami R, Levendis YA, Álvarez L, Gil MV, Pevida C, et al. Single particle

675   ignition and combustion of anthracite, semi-anthracite and bituminous coals in air and

676   simulated oxy-fuel conditions Combustion and Flame 2014,161:1096-1108

677   [19] Zahirović S, Scharler R , Kilpinen P, Obernberger I. Validation of flow simulation and

678   gas combustion sub-models for the CFD-based prediction of NOx formation in biomass grate

679   furnaces. Combustion Theory and Modelling 2010;15: 61-87

680   [20] Bonefacic I, Frankovic B, Kazagic A. Cylindrical particle modelling in pulverized coal

681   and biomass co-firing process. Applied Thermal Engineering 2015;78:74-81

682   [21] Panahi A, Levendis YA, Vorobiev N, Schiemann M. Direct observations on the

683   combustion characteristics of Miscanthus and Beechwood biomass including fusion and

684   spherodization. Fuel Processing Technology 2017;166:41-49

685   [22] Yang Y, Sharifi VN, Swithenbank J, Ma L, Darvell L, Jones JM, Pourkashanian P,

686   Williams A. Combustion of a Single Particle of Biomass. Energy & Fuels 2008; 22:306–316

687   [23] Gubba SR, Ma L, Pourkashanian M, Williams A. Influence of particle shape and

688   internal thermal gradients of biomass particles on pulverised coal/biomass co-fired flames. Fuel

689   Process Technol 2011;92:2185–95.

690   [24] Momeni M, Yin C, Knudsen Kær S, Hvid SL. Comprehensive study of ignition and

691   combustion of single wooden particles. Energy & Fuels 2013;27:1061-1072

692   [25] Lu H, Ip E, Scott J, Foster P, Vickers M, Baxter LL. Effects of particle shape and size

693   on devolatilization of biomass particle. Fuel 2010;89:1156-1168

694   [26] Farazi S, Sadr M, Kang S, Schiemann M, Vorobiev N, Scherer, V, Pitsch H. Resolved

695   simulations of single char particle combustion in a laminar flow field. Fuel 2017;201:15-28

696   [27] Maffei T, Khatami R, Pierucci S, Faravelli T, Ranzi E, Levendis YA. Experimental and

697   modeling study of single coal particle combustion in O2/N2 and Oxy-fuel (O2/CO2)

698   atmospheres. Combustion and Flame 2013;160: 2559-2572

699   [28] Jones JM, Mason PE, Williams A. A compilation of data on the radiant emissivity of

700   some materials at high temperatures, Journal of the Energy Institute, 2018 (in press)

701

702   [29] Magalhães D, Kazanç F, Riaza J, Erensoy S, Kabaklı O Chalmers H. Combustion of

703   Turkish lignites and olive residue: Experiments and kinetic modeling. Fuel 2017;203:868-876

704   [30] Gil MV, Riaza J, Álvarez L, Pevida C, Rubiera F. Biomass devolatilization at high

705   temperature under N2 and CO2: Char morphology and reactivity. Energy 2015;91:655-662

706   [31] Jones JM, Bridgeman TG, Darvell LI, Gudka B, Saddawi A, Williams A. Combustion

707   properties of torrefied willow compared with bituminous coals. Fuel Processing Technology

708   2012;101:1-9

709   [32] Vorobiev N, Becker A, Kruggel-Emden H, Panahi A, Levendis YA, Schiemann M.

710   Particle shape and Stefan flow effects on the burning rate of torrefied biomass. Fuel

711   2017;210:107-120

712   [33] Lu Z, Jian J, Jensen PA, Wu H, Glarborg P. Influence of Torrefaction on Single Particle

713   Combustion of Wood.Energy and Fuels 2016;30:5772-5778

714   [34] Biagini E, Narducci P, Tognotti L. Size and structural characterization of lignin-

715   cellulosic fuels after the rapid devotalization. Fuel 2008;87:177–186

716   [35] Arias B, Pevida C, Fermoso J, Plaza MG, Rubiera F, Pis JJ. Influence of torrefaction

717   on the grindability and reactivity of woody biomass. Fuel Processing Technology 2008;

718   89:169-175

719   [36] Li J, Zhang J. A theoretical study on char combustion of ellipsoidal particles. ()

720   Combustion Science and Technology 2016;188:40-54

721   [37] Tolvanen H, Kokko L, Raiko R. Fast pyrolysis of coal, peat, and torrefied wood: Mass

722   loss study with a drop-tube reactor, particle geometry analysis, and kinetics modeling. Fuel

723   2013;111:148-156

724   [38] Levendis Y, Joshi K, Khatami R, Sarofim A. Combustion behavior in air of single

725   particles from three different coal ranks and from sugarcane bagasse. Combust.

726   Flame 2011;158:452-465

727   [39] Shan L, Kong M, Bennet TD, Sarroza AC, Eastwick C, Sun D, Lu G, Yan Y, Liu H.

728   Studies on combustion behaviours of single biomass particles using a visualization method.

729   Biomass and Bioenergy 2018;109:54-60

730   [40] A. Trubetskaya, P.A. Jensen, A.D. Jensen, M. Steibel, H. Spliethoff, P. Glarborg.

731   Influence of fast pyrolysis conditions on yield and structural transformation of biomass chars.

732   Fuel Process Technol, 140 (2015), pp. 205-214

733

734